IEEE/ASME Transactions on Mechatronics, available online 5 March 2018
DOI: 10.1109/TMECH.2018.2812643

Characterization of Driver Neuromuscular Dynamics for Human-Automation Collaboration Design of Automated Vehicles

Chen Lv, *Member, IEEE*, Huaji Wang, Dongpu Cao, *Member, IEEE*, Yifan Zhao, *Member, IEEE*, Daniel J. Auger, *Senior Member, IEEE*, Mark Sullman, Rebecca Matthias, Lee Skrypchuk, Alexandros Mouzakitis

***Abstract*— In order to design an advanced human-automation collaboration system for highly automated vehicles, research into the driver's neuromuscular dynamics is needed. In this paper a dynamic model of drivers' neuromuscular interaction with a steering wheel is firstly established. The transfer function and the natural frequency of the systems are analyzed. In order to identify the key parameters of the driver-steering-wheel interacting system and investigate the system properties under different situations, experiments with driver-in-the-loop are carried out. For each test subject, two steering tasks, namely the passive and active steering tasks, are instructed to be completed. Furthermore, during the experiments, subjects manipulated the steering wheel with two distinct postures and three different hand positions. Based on the experimental results, key parameters of the transfer function model are identified by using the Gauss-Newton algorithm. Based on the estimated model with identified parameters, investigation of system properties is then carried out. The characteristics of the driver neuromuscular system are discussed and compared with respect to different steering tasks, hand positions and driver postures. These experimental results with identified system properties provide a good foundation for the development of a haptic take-over control system for automated vehicles.**

***Index Terms*—Driver neuromuscular dynamics; driver-vehicle interaction; system identification, automated vehicle; experimental characterization.**

I. Introduction

As one of the typical mechatronics applications in cyber-physical systems, automated vehicle has become an increasingly popular area of interest for both academia and industry [1-6]. Prior to transitioning to fully autonomous driving, highly automated driving will play an important role in the development of automated vehicle technologies [7-9]. We will see cars that are self-driving part of the time but must still be human-driven at other times. For comfort and safety, it is important that there is a smooth and swift transition between the self-driving and human-driving modes [10]. A particular risk is that human drivers may not be ready to take over safely, as they may be preoccupied with non-driving tasks [11, 12]. In this context, one of the critical issues is how to guarantee safe and smooth transitions in the control authority from automated to manual driving [13]. This challenge requires the development of an advanced human-automation collaboration system.

Once the driver perceives a take-over request and returns to the driving task from a non-driving activity, the haptic take-over system will be activated, assisting the driver until manual control is completely resumed [14-17]. During the take-over process it is actually the driver's hand which interacts with the steering wheel, so the driver's neuromuscular dynamics is an important component in the take-over control loop. The control of the haptic take-over system needs to take driver's current muscle state into consideration. Thus, characterization of driver arm's neuromuscular dynamics is an important first step in developing an advanced haptic take-over system.

Driver models with neuromuscular dynamics in vehicle steering control have previously been investigated [18-29]. In [18], the driver's muscles involved in the steering task were identified by measuring muscle activity with electromyography and muscle co-activation during a simulated driving task were observed. Besides, identification of the passive properties of the driver's arms, including inertia, damping and stiffness, were presented. In [19], the function of muscles of the driver's shoulder during vehicle steering maneuver were studied, and relations between electromyography activity of 10 shoulder muscles and driver's steering force were performed. In [20], the muscles involved in generating torque at the steering wheel were firstly identified through experiments, and a mathematical model of the driver's muscle reflex system was established. In [21], a driver model with arm neuromuscular dynamics to investigate driver response to a step angle fault in the active

Chen Lv, Huaji Wang, Yifan Zhao, and Daniel J. Auger, are with the School of Aerospace, Transport and Manufacturing, Cranfield University, Cranfield, Bedford, MK43 0AL, UK (email:{c.lyu, huaji.wang, yifan.zhao, d.j.auger}@cranfield.ac.uk).

Dongpu Cao was with Cranfield University, UK, and he is currently with Mechanical and Mechatronics Engineering, University of Waterloo, ON, N2L 3G1, Canada (e-mail: dongp_ca@yahoo.com) (Corresponding author is D. Cao)

Mark Sullman was with Cranfield University, UK, and he is currently with Middle East Technical University, Cyprus, (email: msullman@metu.edu.tr)

Rebecca Matthias, Lee Skrypchuk and Alexandros Mouzakitis are with Jaguar Land Rover, Coventry, CV3 4LF, UK (email:{rmatthia, lskrypch, amouzakl}@jaguarlandrover.com).

This article has been accepted for publication in a future issue of this journal, but has not been fully edited. Content may change prior to final publication. Citation information: DOI 10.1109/TMECH.2018.2812643, IEEE/ASME Transactions on Mechatronics

front steering system was proposed. In [22], a method was proposed for measuring drivers' steering efficiency during steering maneuvers and evaluating drivers' steering performance and steering comfort. In [23], a mathematical driver model was developed in order to explain the driver steering behavior observed during double lane-change maneuvers. The model consists of a linear quadratic regulator path-following controller coupled to a neuromuscular system. Nevertheless, the existing studies have mostly been in relation to manual driving and conventional vehicle dynamics control, rather than targeting the driver-automation collaboration system design for highly automated vehicles.

This paper aims to research the neuromuscular dynamics in relation to haptic take-over system design for automated vehicles. And the presented study can be the foundation for designing not only the driver-vehicle interaction system of highly automated vehicles, but also other advanced driver assistance systems with different levels of automation. The main contribution of this paper lies in the following aspects: (1) The model of driver neuromuscular dynamics interacting with a steering wheel is established; (2) Identification and characterization of the driver-vehicle system are carried out with experimental data collected under different testing conditions; (3) The developed driver-vehicle system model with characteristics analyzed could help to set up a solid foundation for future studies in take-over controller synthesis for driver-automation collaboration.

The rest of the article is organized as follows. The model of driver neuromuscular dynamics, while interacting with a steering wheel, is firstly established in Section II. The system identification of the transfer function model is formulated as a nonlinear least squares problem in Section III, and the Gauss-Newton algorithm is adopted for solving it. Section IV presents the experiment design with introduction of steering tasks, driver postures, hand positions, and data measurement and acquisition. Experimental data with system identification results are presented in Section V. Characterization of the drivers' neuromuscular system are analyzed and discussed in Section VI, which is followed by the concluding remarks in Section VII.

II. Dynamic Model of The Driver-Steering-Wheel Interacting System

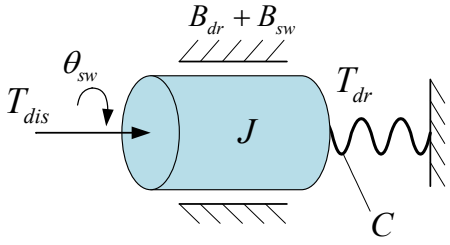

Fig. 1. The simplified inertia model for the driver-steering-wheel interacting system.

In order to investigate the characteristics of the driver's neuromuscular system, during interaction with the steering wheel, the driver-vehicle interacting system model must firstly be established. The driver-steering-wheel interaction system is comprised of a steering wheel and the driver's neuromuscular system. Fig. 1 shows a simplified single-inertia model of the driver-steering-wheel interacting system. It is abstracted from the physical structure with its main damping and stiffness properties [16].

There are two degrees of freedom in the driver-steering-wheel interacting system (described above), namely the steering column angle and the steering wheel angle. The output torque of the electric power steering (EPS) motor is considered as a disturbance to the driver, and the driver adds additional inertia J_{dr}, damping B_{dr} and stiffness C to the steering wheel. Thus, according to the above developed model, the dynamic equation for the driver-steering-wheel interacting system can be represented as follows:

$$T_{dr} - T_{dis} = J\ddot{\theta}_{sw} + B\dot{\theta}_{sw} + C\theta_{sw} \tag{1}$$

$$T_{dis} = T_{mot,tgt} \tag{2}$$

$$J = J_{dr} + J_{sw}, \quad B = B_{dr} + B_{sw} \tag{3}$$

where T_{dr} is the driver's steering torque, T_{dis} is the disturbance torque, $T_{\mathrm{mot,tgt}}$ is the target torque of the steering motor, and T_{dis}= $T_{\mathrm{mot,tgt}}$. C is the stiffness coefficient of the interacting system, and θ_{sw} is the steering angle. J is the lumped inertia, J_{dr} is the driver arm's inertia, J_{sw} is the inertia of the steering wheel, B_{dr} and $\mathrm{B_{sw}}$ are the viscous damping terms of driver's neuromuscular system and steering wheel bearings, respectively, and B is the lumped viscous coefficient.

According to the above established dynamic model, the transfer function of the driver-steering-wheel interacting system can be developed, as shown in the Eq. (4).

$$\frac{\theta_{sw}}{T_{dr}} = \frac{1}{Js^2 + Bs + C} \tag{4}$$

Based on this equation (4), the natural frequency Ω of the driver-steering-wheel interacting system can be derived as:

$$\Omega = \frac{1}{2\pi}\sqrt{(1-\xi^2)\frac{C}{J}} \tag{5}$$

where ξ is the damping ratio.

Thus, in order to achieve the characterization of driver neuromuscular dynamics during interaction with a steering wheel, the above transfer functions with the values of the key parameters need to be identified.

III. System Identification Methodology

In this study, the system identification of the transfer function model is formulated as a nonlinear least squares problem, with adopted algorithms introduced as follows.

A. Nonlinear Least Squares Problem

The nonlinear least squares problem aims at finding an optimal set of parameters for the model given a large set of data [30]. Given a set of measured data (t_j, y_j) and a model function $\phi(x, t_j)$ with the input variables of $x_1 \ldots x_n$, the discrepancy

This article has been accepted for publication in a future issue of this journal, but has not been fully edited. Content may change prior to final publication. Citation information: DOI 10.1109/TMECH.2018.2812643, IEEE/ASME Transactions on Mechatronics

between the model function and the measured data can be represented by the residual r_j:

$$r_j(x) = y_j - \phi(x, t_j) \tag{6}$$

where y_j is y component of the data point at t_j.

The objective function can be chosen as:

$$f(x) = \frac{1}{2}\sum_{j=1}^{m} r_j^2(x) \tag{7}$$

Considering the residual vector r which is comprised of all components r_j (j=1,…m), where m is the number of samples, the Jacobian matrix can be given by (m>n):

$$J(x) := \begin{bmatrix} \frac{\partial r_1}{\partial x_1} & \cdots & \frac{\partial r_1}{\partial x_n} \\ \vdots & & \vdots \\ \frac{\partial r_m}{\partial x_1} & \cdots & \frac{\partial r_m}{\partial x_n} \end{bmatrix} \tag{8}$$

Combing Eq. (6)-(8), the gradient and the Hessian of the objective function can be calculated in terms of the Jacobian:

$$\nabla f(x) = \sum_{j=1}^{m} r_j(x)\frac{\partial r_j}{\partial x_i} = J^T(x)r(x) \tag{9}$$

$$\begin{aligned} \nabla^2 f(x) &= \sum_{j=1}^{m}\frac{\partial r_j}{\partial x_k}\frac{\partial r_j}{\partial x_i} + \sum_{j=1}^{m} r_j \frac{\partial^2 r_j}{\partial x_i \partial x_k} \\ &= J^T(x)J(x) + \sum_{j=1}^{n} r_j(x)\nabla^2 r_j(x) \end{aligned} \tag{10}$$

In the above Eq. (10), because the residuals r_j are small and the model ϕ(x, t) is considered to be nearly linear in x, thus the second term of Eq. (10) is assumed to be small and is neglected.

B. The Gauss-Newton Algorithm

In order to solve the above formulated nonlinear least squares problem, the Gauss-Newton (GN) algorithm is adopted. It is a quasi-Newton method using a search direction vector p_k^{GN} and a step size a_k as [31]:

$$x_{k+1} = x_k + \alpha_k p_k \tag{11}$$

In the iteration process of GN algorithm, the above Eq. (11) is repeatedly implemented until the model function fits the data points satisfactorily.

The Hessian can be approximated to be $J_k^T J_k$, thus the search direction p^{GN} can be given by

$$J_k^T J_k p_k^{GN} = -J_k^T r_k \tag{12}$$

The GN direction p_k^{GN} is the solution of the linear least squares problem

$$\min_p \left\| J_k p + r_k \right\| \tag{13}$$

Whenever J_k has full rank, the search direction is a descent direction, which can be proved as

$$\begin{aligned} \nabla f_k^T p_k^{GN} &= (J_k^T r_k)^T p_k^{GN} \\ &= -(J_k^T J_k p^{GN})^T p_k^{GN} \\ &= -(p_k^{GN})^T J_k^T J_k p_k^{GN} \\ &= -\left\| J_k p_k^{GN} \right\|^2 \le 0 \end{aligned} \tag{14}$$

The above equality condition takes place if and only if $J_k p_k^{GN} = 0$, i.e. $J_k^T r_k = \nabla f_k = 0$, indicating that x_k is a stationary point and no further iterations are necessary.

After the GN direction is found, the step length a_k for each iteration is required to be determined. It can be computed by minimizing the model function $\phi(x, t)$ at the new point $x_k + a_k p_k$ with respect to the variable a_k (where a_k>0). So as to find the optimal step length, a_k can be chosen such that

$$\phi(x_k + \alpha_k p_k^{GN}) \le \phi(x_k) + c_1 \alpha_k \nabla\phi(x_k) p_k^{GN} \tag{15}$$

where c_1 is a constant with the condition $0 < c_1 < 1$.

C. Convergence Analysis of the GN Algorithm

The stability of the GN Algorithm is investigated with the convergence property analyzed in this section. The following theorem demonstrates sufficient conditions for the GN method to converge a point such that $\nabla f = J^T r = 0$.

Theorem 1. [32] *Suppose that each residual function r_j is Lipschitz continuously differentiable in a neighborhood of the level set*

$$L := \{x \ : \ f(x) \le f(x_0)\} \tag{16}$$

and the Jacobian satisfies the condition of uniform full-rank

$$\left\| J(x)z \right\| \ge \gamma \left\| z \right\|. \tag{17}$$

Then if the iterates x_k which are generated by the Gauss-Newton method with the step lengths satisfy the Wolfe conditions, we obtain

$$\lim_{k\to\infty} J_k^T r_k = 0. \tag{18}$$

Proof. The Gauss-Newton is a line search quasi-Newton method. Lipschitz continuity of ∇r_j indicates Lipschitz continuity of ∇f over the neighborhood of L. Hence, we obtain all assumptions which are sufficient for the Zoutendijk condition to hold. Thus, it can be deduced that cos θ_k, k = 0, 1, 2,…, are uniformly bounded away from zero.

Since Lipschitz continuity of each ∇r_j implies the continuity of $J(x)$, thus there is a constant $\beta > 0$ such that

$$\left\| J(x) \right\| \ge \beta, \quad x \in L. \tag{19}$$

Then, we have

This article has been accepted for publication in a future issue of this journal, but has not been fully edited. Content may change prior to final publication. Citation information: DOI 10.1109/TMECH.2018.2812643, IEEE/ASME Transactions on Mechatronics

$$\begin{aligned}\cos\theta_k &= -\frac{\nabla f^T p^{GN}}{\|\nabla f\|\|p^{GN}\|} = \frac{r^T J p^{GN}}{\|J^T r\|\|p^{GN}\|} \\ &= \frac{\|Jp^{GN}\|^2}{\|J^T Jp^{GN}\|\|p^{GN}\|} \geq \frac{\gamma^2\|p^{GN}\|^2}{\beta^2\|p^{GN}\|^2} \\ &= \frac{\gamma^2}{\beta^2} > 0.\end{aligned} \tag{20}$$

The rate of convergence is now analyzed as follows. Suppose x^* is a local minimum point such that $\nabla f(x^*) = 0$, then

$$\begin{aligned}x_{k+1} - x^* &= x_k + p_k^{GN} - x^* \\ &= x_k - x^* - [J_k^T J_k]^{-1}\nabla f_k \\ &= [J_k^T J_k]^{-1}\left[[J_k^T J_k](x_k - x^*) + \nabla f^* - \nabla f_k\right]\end{aligned} \tag{21}$$

Here we introduce the notation for the Hessian of f as follows

$$\begin{aligned}\nabla^2 f(x) &= J^T(x)J(x) + \sum_{j=1}^{n} r_j(x)\nabla^2 r_j(x) \\ &= J^T(x)J(x) + H(x)\end{aligned} \tag{22}$$

Then we have

$$\begin{aligned}\nabla f_k - \nabla f^* &= \int_0^1 J^T J(x^* + t(x_k - x^*))(x_k - x^*)dt \\ &+ \int_0^1 H(x^* + t(x_k - x^*))(x_k - x^*)dt\end{aligned} \tag{23}$$

Assume that $J^T J(x^*)$ is invertible and J is Lipschitz-continuous, then for all $x \in B_1^\varepsilon$ with any $\varepsilon > 0$, there is a spherical space B_1^ε around x^* such that

$$\left\|[J^T J(x)]^{-1}\right\| \leq (1+\varepsilon)\left\|[J^T J(x^*)]^{-1}\right\| < \infty \tag{24}$$

where $x \in B_1^\varepsilon$.

Moreover, let's assume that H is continuous, then for all $x \in B_2^\varepsilon$, there is another spherical space B_2^ε around x^* such that

$$\|H(x)\| \leq (1+\varepsilon)\|H(x^*)\| \tag{25}$$

If $x \in B_1^\varepsilon \cap B_2^\varepsilon$, then we obtain

$$\begin{aligned}\|x_{k+1} - x^*\| &= \Big\|[J^T J(x_k)]^{-1}\Big\{J^T J(x_k)(x_k - x^*) \\ &+ \int_0^1 J^T J(x^* + t(x_k - x^*))(x_k - x^*)dt \\ &+ \int_0^1 H(x^* + t(x_k - x^*))(x_k - x^*)dt\Big\}\Big\| \\ &\leq \int_0^1 \left\|[J^T J(x_k)]^{-1} H(x^* + t(x_k - x^*))\right\|\|x_k - x^*\|dt \\ &+ O(\|x_k - x^*\|^2) \\ &\leq (1+\varepsilon)^2\left\|[J^T J(x^*)]^{-1} H(x^*)\right\|\|x_k - x^*\| \\ &+ O(\|x_k - x^*\|^2)\end{aligned} \tag{26}$$

Thus, the convergence rate of the Gauss-Newton method is determined by the value of $\left\|[J^T J(x^*)]^{-1} H(x^*)\right\|$. So as to obtain that $\|x_k + p^{GN} - x^*\| < \|x_k - x^*\|$, i.e. the GN step of unit length gets closer to the solution, the following condition needs to be achieved

$$\left\|[J^T J(x^*)]^{-1} H(x^*)\right\| < 1 \tag{27}$$

With small residual in a nearly linear condition, we have

$$\left\|[J^T J(x^*)]^{-1} H(x^*)\right\| << 1 \tag{28}$$

hence, the rapid convergence can be achieved. Moreover, if $H(x^*) = 0$, then the convergence is quadratic.

IV. Experiment Design and Data Collection

In order to identify transfer functions with the values of the key parameters of the driver-steering-wheel interacting system and investigate system properties under different driving tasks and situations, a large set of data are obtained through driver-in-the-loop experiments [19, 22]. There are two types of the experiments that need to be completed by each test subject, i.e. the active and passive steering tasks. During experiments, the test subjects sit on the seat of a driving simulator and they are instructed to manipulate the steering wheel using their right arm and both arms with distinct gripping positions, respectively. These tested postures and hand positions are abstracted from comprehensive investigations of driver behavior in daily driving scenarios. The detailed steering tasks, driver posture and hand positions are described as follows.

A. Steering Tasks

The test subject is required to carry out two steering tasks: passive steering and active steering [16].

1) Passive steering task: The subject is instructed to stabilize the steering wheel at its neutral position under the disturbed torque produced by the EPS motor. The magnitude and frequency of the disturbed torque are set at 5 Nm and 0.025 Hz, respectively.

The magnitude of the disturbed torque is determined by referring to the value of the resistant torque in the actual driving conditions with a typical power-assisted steering system. The frequency of the disturbed torque is determined in a quasi-steady range in order to identify distinct and useful results. During tests, the subject is required to continuously stabilize the steering wheel, keeping it at its neutral position against the varied disturbance torque.

2) Active steering task: The subject is instructed to perform a sine-wave steering angle, to mimic the slalom steering test. The magnitude and frequency of the sine-wave steering angle are set at around 60 degrees and 0.25 Hz, respectively. During this test the EPS motor will work and provide assistant power to the driver. The subject needs to perform the above sine-wave steering operation continually for at least 5 cycles.

B. Driver Posture and Hand Positions

To simulate the typical driving situation, the test subjects are

This article has been accepted for publication in a future issue of this journal, but has not been fully edited. Content may change prior to final publication. Citation information: DOI 10.1109/TMECH.2018.2812643, IEEE/ASME Transactions on Mechatronics

required to sit in the seat of a driving simulator and slightly bend their elbows with an angle of 110 degrees between the forearm and upper arm. The steering wheel is adjusted to ensure that the line along the steering axis is parallel to the line through the shoulder and wrist joints. Furthermore, during the experiments the subjects are required to manipulate the steering wheel with two distinct postures and three different hand positions [16]. The detailed driver postures and hand positions are introduced as follows.

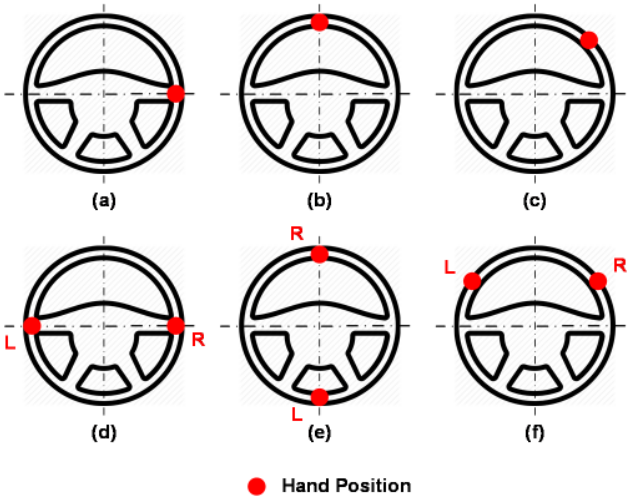

Fig. 2. Illustration of the six distinct hand positions.

1) Right arm only with three hand positions: In this scenario, the driver operates the steering wheel using the right arm only, and the left hand is held away from the steering wheel. The three gripping positions are the 3 o'clock position, 12 o'clock position and 1:30 position, which correspond to the subplots (a), (b), (c) in Fig. 2, respectively. The test subjects are required to grasp the steering wheel at the locations of the hour hand, which points to the above mentioned time in order to complete the driving tasks (see Fig. 2).

2) Both arms with three hand positions: In this scenario, the driver uses the steering wheel with both arms. There are three gripping positions on the steering wheel, which were the: 3 and 9 o'clock position, 12 and 6 o'clock position and 10:10 position. The positions of the 3 and 9 o'clock and 12 and 6 o'clock indicate that the test subjects are required to grasp the steering wheel at the locations of the above times using one hand for each. For the 10:10 position, the left and right hands of the subject are placed at the locations of the hour and ten past the hour on a clock, respectively. A schematic diagram of the above hand positions are illustrated in subplots of (d), (e), (f) in Fig. 2, respectively. Each test subject completed both the active and passive steering tasks in all six hand positions.

C. Data Measurement and Acquisition

During steering the force exerted by the driver on the steering wheel can be divided into two parts: the force which is perpendicular to the wheel plane and the force in the wheel plane. Moreover, the force applied in the wheel plane at the grasping point can be further divided into two components: the radial resultant force and the tangential force. The force perpendicular to the wheel plane and the radial force in the wheel plane are the assistant forces to maintain the body's stability and the balance of the driver when steering, but are not able to generate a steering moment to rotate the wheel. Only the

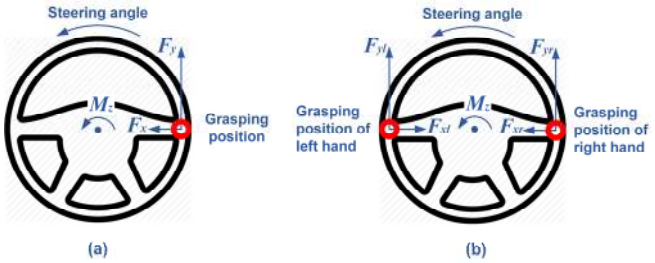

Fig. 3. Illustration of the forces and steering torque generated at different grasping positions.

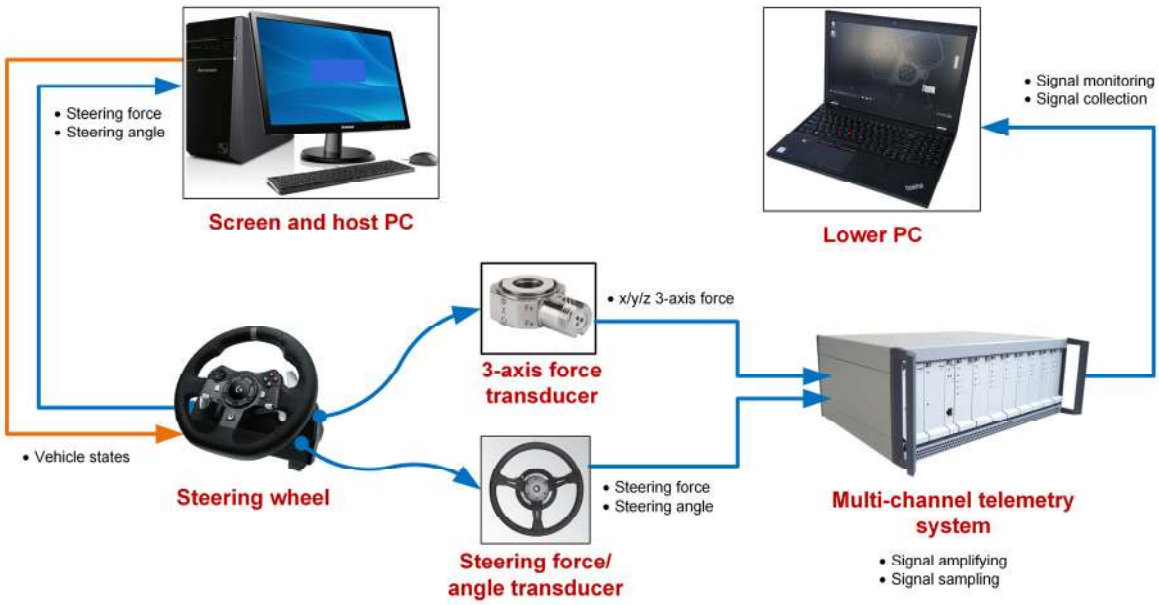

Fig. 4. Overall structure of the experimental environment.

This article has been accepted for publication in a future issue of this journal, but has not been fully edited. Content may change prior to final publication. Citation information: DOI 10.1109/TMECH.2018.2812643, IEEE/ASME Transactions on Mechatronics

tangential force contributes to the steering moment. And the measured steering moment M_z is equal to driver's input steering torque T_{dr}.

In order to measure the applied force in the wheel plane, the coordinate system, with its origin at the point of grasping point, is firstly established. Fig. 3 (a) and (b) illustrate the forces and steering torque generated by right arm only with the 3 o'clock grasping position and by both arms with the 3 and 9 o'clock position, respectively. F_y is in the longitudinal direction of the vehicle, pointing forwards, and F_x is in the lateral direction. Take the 3 o'clock grasping position illustrated in Fig. 3 (a) as an example. The measured tangential force F_y generates the steering moment M_z that steers the vehicle, while the radial force F_x, which is towards the center of the steering plane, is not related to the generated moment around the steering column.

The forces applied by the subject's hands are measured by a 3-axis force transducer, and the steering angle and steering torque are measured using a steering angle/force sensor with the sampling frequency of 1000 Hz. These forces, steering angle and torque were firstly amplified and then sampled with 100 Hz by a multi-channel telemetric equipment. The overall structure of the experimental devices is shown in Fig. 4.

V. Experiment Results

Using the above procedure and methodology, steering experiments are carried out in the driving simulator. In the tests, ten drivers with natural driving experience and skills are selected as experimental subjects and neuromuscular dynamics data are collected. The results of different steering tasks with distinct driver postures and hand positions are reported as follows.

A. Experimental Data of the Passive Steering Task

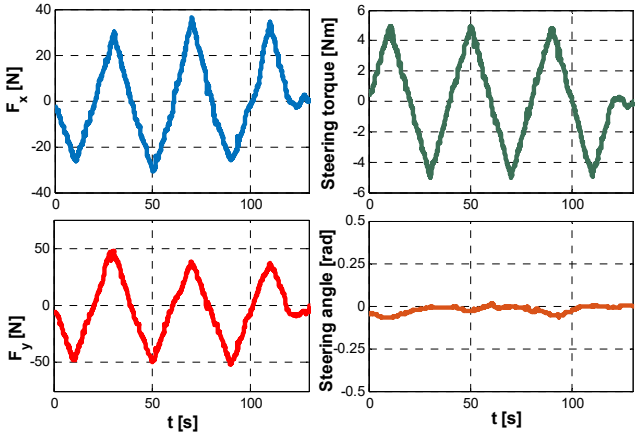

Fig. 5. Experimental data from the passive steering task, right arm only at the 1:30 grasping position.

Fig. 5 shows an example of the test data resulting from the passive steering task using only the right arm at the 1:30 grasping position. As described in section III, the test subject is required to keep the steering wheel at the neutral position against the disturbance torque generated by the EPS motor. According to Fig. 5, the external disturbance torque is generated as a triangle wave with 10 Nm of peak to peak amplitude and 0.025 Hz of frequency. Then the driver operates the steering wheel, which can be indicated by the variation in the applied forces F_x and F_y, as well as the tangential force in a steering moment on the steering plane. Thus, the steering torque is detected, as shown in Fig. 5. As a result, the value of the steering angle remains within a small range around 0 rad.

B. Experimental Data of the Active Steering Task

Fig. 6 shows an example of the test data generated by active steering with the right arm only at the 3 o'clock hand position. As described in section III, the test subject is required to steer the wheel as a sine wave with the angle of around 1.0 rad (i.e. 60 degrees) and the frequency of 0.25 Hz.

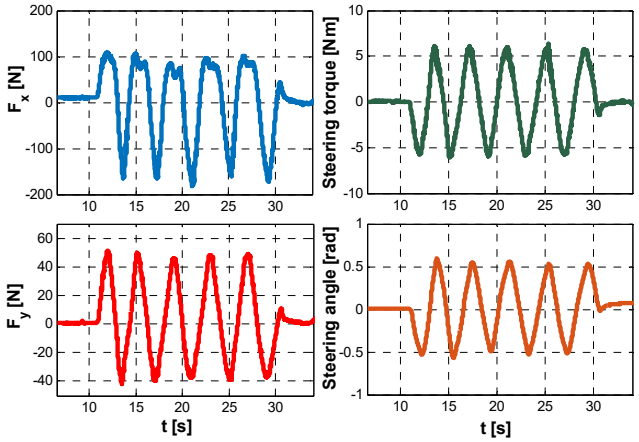

Fig. 6. Experimental data from the active steering task with right arm only at the 3 o'clock hand position.

According to the results shown in Fig. 6, the driver operates the steering wheel by applying forces F_x and F_y. The resultant tangential force on the steering plane generates a steering moment, and then the steering torque is detected. As a result, the measured steering angle presents a sine wave style with the amplitude at 0.5 rad and the frequency of 0.25 Hz.

C. System Identification and Model Validation

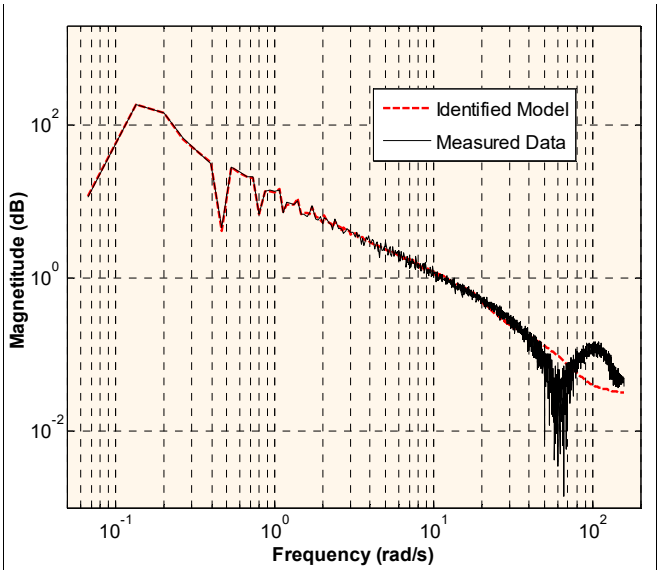

Fig. 7. Comparison of the amplitude curves of the data's and the models' frequency responses.

This article has been accepted for publication in a future issue of this journal, but has not been fully edited. Content may change prior to final publication. Citation information: DOI 10.1109/TMECH.2018.2812643, IEEE/ASME Transactions on Mechatronics

In order to validate the effectiveness and accuracy of the identified system model, the output of the model is compared with the measured data in the frequency domain. The identified model is fed with inputs from the measured data set, then the amplitude of the model output can be derived by using the input Fourier Transform times the model's frequency function.

Fig. 7 shows an example of the comparison of the amplitude curves of the data's and the models' frequency responses (active steering task with right arm only at the 3 o'clock hand position). According to the results, the overall accuracy of the estimated model is over 97%, and within the particular frequency range under 5 Hz, which covers the main working range of the system [19, 22, 25], the amplitude of the model output fits the measured output's amplitude perfectly.

VI. Results Analysis and Discussion

The characteristics of the drivers' neuromuscular system are analyzed and compared with respect to the different steering tasks, hand positions and driver postures.

A. Comparison of the Results with Passive and Active Steering Tasks

The values of the moment of inertia, the stiffness coefficient, and the natural frequency of the driver-steering-wheel interacting system for the active and passive steering tasks are compared.

1) The moment of inertia of the interacting system: According to the system parameter identification results, the values of the moment of inertia of the driver-steering-wheel interacting system under the passive and active steering tasks are compared as follows.

Based on the results of the identified moment of inertia collected from the ten subjects, the nominal value of the moment of inertia for the subjects is of 0.11 Nm/(rad/s^2)， and the real value varies slightly from 0.03 to 0.18 Nm/(rad/s^2). For each subject there is no evident variation in the values of the parameters for the different steering tasks. The reason for the phenomena observed above is because the moment of inertia depends on the distribution of mass with respect to the axis of rotation. During different steering tasks the mass distribution of the driver's arm and the steering wheel around the steering axis (steering column) shows little change. Thus, the value of the moment of inertia is not closely correlated to the passive or active steering tasks.

2) The stiffness coefficient of the interacting system: According to the parameter identification results, the correlation of the stiffness coefficient of the driver-steering-wheel interacting system, with the passive and active steering tasks, are analyzed as follows.

Fig. 8 presents the stiffness coefficient from the ten subjects in the passive and active steering tasks. The maximum value of the stiffness coefficient among the ten subjects reaches over 80 Nm/rad in the passive condition, while the minimum value is below 5 Nm/rad in the active condition. It can clearly be seen that the values of the stiffness coefficient in the passive steering scenarios are much larger than those in the active steering modes. A reasonable explanation for the above results is that the driver's arm is tensed in order to stabilize the steering wheel against the disturbed torque in the passive mode, and the represented stiffness coefficient of the system is therefore increased due to the co-contraction effect of the muscles.

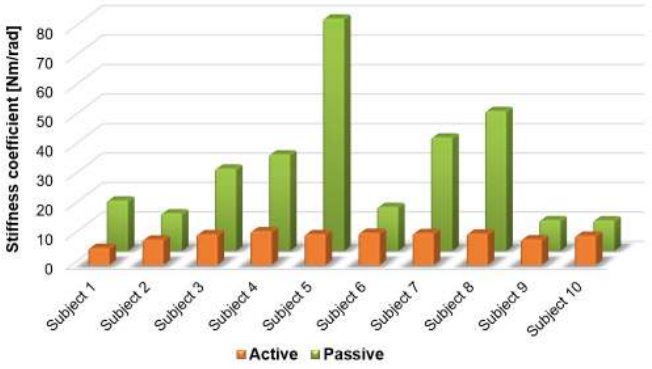

Fig. 8. The results of the stiffness coefficient of the ten subjects under passive and active steering tasks.

3) Natural frequency of the interacting system: The values of the natural frequency of the driver-steering-wheel interacting system under active and passive steering tasks are compared as follows.

Fig. 9 presents the natural frequency of the ten subjects under passive and active steering tasks. This shows that the values of the natural frequency under the passive steering task are much larger than those in the active steering tasks. In the passive conditions, the values of the stiffness coefficient of the ten subjects are mainly within the range of 2.5Hz-3.5Hz, and the values under the active steering tasks are mostly below 1 Hz. This is because that the natural frequency of the system is positively correlated with the stiffness coefficient. When the stiffness coefficient increases in the passive steering conditions, the natural frequency accordingly becomes larger.

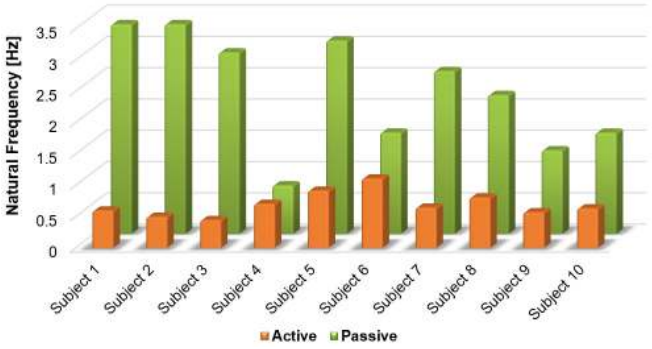

Fig. 9. Results of the natural frequency of the ten subjects under the passive and active steering tasks.

Table I shows detailed identification results of data from ten subjects under the passive steering task using the right arm only with hand positions at 3 o'clock, 12 o'clock and 1:30. And detailed identification results from ten subjects in the active steering task, using the right arm only, with hands in the 3 o'clock, 12 o'clock and 1:30 positions are presented in Table II.

B. Comparison of the Results with Different Hand Positions

The test results presented in Tables I and II show no evident variation in the values of the moment of inertia, the stiffness

This article has been accepted for publication in a future issue of this journal, but has not been fully edited. Content may change prior to final publication. Citation information: DOI 10.1109/TMECH.2018.2812643, IEEE/ASME Transactions on Mechatronics

TABLE I.
IDENTIFICATION RESULTS OF DATA FROM SUBJECTS IN THE PASSIVE STEERING TASK (RIGHT ARM ONLY) WITH THREE HAND POSITIONS

Hand Position	*J* Nm/(rad/s²)]		*B* [Nm/(rad/s)]		*C* [Nm/rad]		*f* [Hz]	
	Nominal Value	Value Range	Nominal Value	Value Range	Nominal Value	Value Range	Nominal Value	Value Range
3	0.11	[0.03 0.14]	1.5	[0.1 2.5]	22.7	[13.8 69.5]	3.3	[0.85 4.11]
12	0.11	[0.03 0.18]	2.1	[0.1 4.1]	45.9	[29.1 80.5]	2.8	[0.82 4.24]
130	0.11	[0.05 0.14]	0.7	[0.1 3.1]	17.0	[13.0 35.2]	3.1	[0.95 4.27]

TABLE II.
IDENTIFICATION RESULTS OF DATA FROM SUBJECTS IN THE ACTIVE STEERING TASK (RIGHT ARM ONLY) WITH THREE HAND POSITIONS

Hand Position	*J* [Nm/(rad/s²)]		*B* [Nm/(rad/s)]		*C* [Nm/rad]		*f* [Hz]	
	Nominal Value	Value Range	Nominal Value	Value Range	Nominal Value	Value Range	Nominal Value	Value Range
3	0.11	[0.03 0.17]	2.9	[1.2 3.6]	10.2	[5.1 12.1]	0.8	[0.52 1.36]
12	0.11	[0.03 0.18]	3.0	[1.6 4.4]	9.2	[4.5 13.1]	0.7	[0.34 1.19]
130	0.11	[0.02 0.17]	3.1	[2.4 3.4]	10.0	[7.8 11.1]	0.8	[0.37 1.03]

coefficient, and the natural frequency of the driver-steering-wheel interacting system, with respect to the three different hand positions.

C. Comparison of the Results with Different Postures

According to experimental results with different postures, the value of the identified moment of inertia increases under the conditions of steering with both arms, compared to steering with the right arm only. This is because by using both arms the mass distribution of the system around the steering axis becomes larger. In the meantime, both the values of the natural frequency and system stiffness coefficient increase when steering with both arms.

D. Correlation Analysis

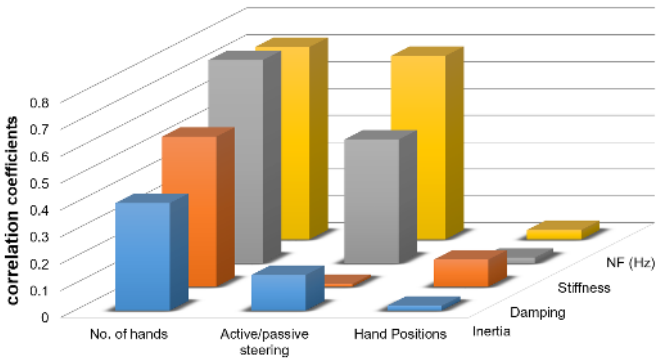

Fig. 10. The results of the correlations between the labels of the measured data and the key parameters of the estimated system model.

The correlations between the multiple labels of the collected data and parameters of the estimated transfer function model are further analyzed. The labels of the data that are collected during the experiments include the number of hands used for steering, the active/passive steering mode, and the hand positions, while the parameters of the identified system model include the inertia, the damping coefficient, the stiffness coefficient, and the natural frequency of the driver-steering-wheel system.

Based on the results shown in Fig. 10, the number of hands, active/passive steering mode are significantly correlated with the stiffness coefficient and natural frequency of the system. However, hand positions have little impact on system's transfer function.

VII. CONCLUSIONS AND FUTURE WORK

This paper investigates the characterization of driver neuromuscular dynamics for haptic take-over system design in automated vehicles. The model of driver neuromuscular dynamics during interaction with a steering wheel is established. The transfer function and the natural frequency of the system are analyzed. To investigate the key parameters and properties of the system, experiments with driver-in-the-loop are carried out under different situations. Based on the test results, the values of the stiffness coefficient in the passive steering modes are much larger than those in the active steering ones. And the values of the stiffness coefficient of the subjects are mainly within the range of 2.5Hz-3.5Hz, and the values under the active steering tasks are mostly below 1 Hz. Besides, the value of the identified moment of inertia increases under the conditions of steering with both arms, compared to steering with the right arm only. However, there is no evident variation

in the values of the moment of inertia, the stiffness coefficient, and the natural frequency, with respect to the three different hand positions. These results and system properties identified in this research will help to provide a foundation for the development of the haptic take-over control system for automated vehicles.

Further work can be carried out in the following areas: robust online identification algorithm of driver neuromuscular dynamics will be developed; approach for driver take-over capability assessment will be established based on driver neuromuscular state observation; control algorithms of haptic feedback torque will be designed based on driver neuromuscular dynamics.

ACKNOWLEDGMENT

This work was supported by Jaguar Land Rover and the UK-EPSRC grant EP/ N012089/1 as part of the jointly funded Towards Autonomy: Smart and Connected Control (TASCC) Program.

REFERENCES

[1] F.-Y. Wang, "Control 5.0: from Newton to Merton in popper's cyber-social-physical spaces," IEEE/CAA Journal of Automatica Sinica, vol. 3, pp. 233-234, 2016.

[2] Bisoffi, A., Biral, F., Da Lio, M. and Zaccarian, L. Longitudinal Jerk Estimation of Driver Intentions for Advanced Driver Assistance Systems. IEEE/ASME Transactions on Mechatronics, 22(4), pp.1531-1541, 2017.

[3] Lv, C., Liu, Y., Hu, X., Guo, H., Cao, D. and Wang, F.Y. Simultaneous Observation of Hybrid States for Cyber-Physical Systems: A Case Study of Electric Vehicle Powertrain. IEEE Transactions on Cybernetics, 2017.

[4] G. Xie, H. Gao, L. Qian, B. Huang, K. Li, and J. Wang, "Vehicle Trajectory Prediction by Integrating Physics- and Maneuver-based Approaches Using Interactive Multiple Models," IEEE Transactions on Industrial Electronics, 2017, in press.

[5] C. Lv, Y. Xing, J. Zhang, X. Na, Y. Li, T. Liu, et al., "Levenberg-Marquardt Backpropagation Training of Multilayer Neural Networks for State Estimation of A Safety Critical Cyber-Physical System," IEEE Transactions on Industrial Informatics, 2017, in press.

[6] C. Lv, H. Wang, and D. Cao, "High-Precision Hydraulic Pressure Control Based on Linear Pressure-Drop Modulation in Valve Critical Equilibrium State," IEEE Transactions on Industrial Electronics, vol. 64, pp. 7984-7993, 2017.

[7] Gao, H. B., X. Y. Zhang, T. L. Zhang, Y. Liu, and D. Li. "Research of intelligent vehicle variable granularity evaluation based on cloud model." Acta Electronica Sinica 44, no. 2 (2016): 365-373.

[8] Zhang, X., Gao, H., et al. "Multi-view clustering based on graph-regularized nonnegative matrix factorization for object recognition." Information Sciences (2017).

[9] Lv, C., Wang, H., Zhao, B., Cao, D., Huaji, W., Zhang, J., Li, Y. and Yuan, Y. Cyber-Physical System Based Optimization Framework for Intelligent Powertrain Control. SAE International Journal of Commercial Vehicles, 10(2017-01-0426), pp.254-264, 2017.

[10] B. Mok, M. Johns, N. Gowda, S. Sibi, and W. Ju, "Take the wheel: Effects of available modalities on driver intervention," in 2016 IEEE Intelligent Vehicles Symposium (IV), 2016, pp. 1358-1365.

[11] Y. Xing, C. Lv, Z. Zhang, H. Wang, X. Na, D. Cao, et al., "Identification and Analysis of Driver Postures for In-Vehicle Driving Activities and Secondary Tasks Recognition," IEEE Transactions on Computational Social Systems, 2017, in press.

[12] Xing, Y., Lv, C., Cao, D., Wang, H. and Zhao, Y., "Driver workload estimation using a novel hybrid method of error reduction ratio causality and support vector machine." Measurement 114 (2018): 390-397.

[13] H. E. Russell, L. K. Harbott, I. Nisky, S. Pan, A. M. Okamura, and J. C. Gerdes, "Motor learning affects car-to-driver handover in automated vehicles," Science Robotics, vol. 1, p. eaah5682, 2016.

[14] C. Lv, D. Cao, Y. Zhao, D. J. Auger, M. Sullman, H. Wang, et al., "Analysis of autopilot disengagements occurring during autonomous vehicle testing," IEEE/CAA Journal of Automatica Sinica, vol. 5, pp. 58-68, 2018.

[15] C. J. Ploch, J. H. Bae, C. C. Ploch, W. Ju, and M. R. Cutkosky, "Comparing haptic and audio navigation cues on the road for distracted drivers with a skin stretch steering wheel," in 2017 IEEE World Haptics Conference (WHC), 2017, pp. 448-453.

[16] C. Lv, H. Wang, D. Cao, Y. Zhao, D. J. Auger, M. Sullman, et al., "Characterisation of driver neuromuscular dynamics for haptic take-over system design for automated vehicles," in IECON 2017 - 43rd Annual Conference of the IEEE Industrial Electronics Society, 2017, pp. 4565-4570.

[17] Katzourakis, D.I., Lazic, N., Olsson, C. and Lidberg, M.R. Driver steering override for lane-keeping aid using computer-aided engineering. IEEE/ASME Transactions on Mechatronics, 20(4), pp.1543-1552, 2015.

[18] A. Pick and D. Cole, "Neuromuscular dynamics and the vehicle steering task," The Dynamics of Vehicles on Roads and on Tracks, vol. 41, pp. 182-191, 2003.

[19] Y. Liu, X. Ji, H. Ryouhei, M. Takahiro, and L. Lou, "Function of shoulder muscles of driver in vehicle steering maneuver," Science China Technological Sciences, vol. 55, pp. 3445-3454, 2012.

[20] A. Pick and D. Cole, "Neuromuscular dynamics in the driver–vehicle system," Vehicle system dynamics, vol. 44, pp. 624-631, 2006.

[21] D. Cole. "A path-following driver–vehicle model with neuromuscular dynamics, including measured and simulated responses to a step in steering angle overlay." Vehicle system dynamics 50, no. 4: 573-596, 2012.

[22] Y. Liu, X. Ji, R. Hayama, T. Mizuno, and S. Nakano, "Method for measuring a driver's steering efficiency using electromyography," Proceedings of the Institution of Mechanical Engineers, Part D: Journal of Automobile Engineering, vol. 228, pp. 1170-1184, 2014.

[23] A. J. Pick and D. J. Cole, "A mathematical model of driver steering control including neuromuscular dynamics," Journal of Dynamic Systems, Measurement, and Control, vol. 130, p. 031004, 2008.

[24] T. Qu, H. Chen, D. Cao, H. Guo, and B. Gao, "Switching-based stochastic model predictive control approach for modeling driver steering skill," IEEE Transactions on Intelligent Transportation Systems, vol. 16, pp. 365-375, 2015.

[25] Liu, Y., Ji, X., Hayama, R. and Mizuno, T., "A novel estimating method for steering efficiency of the driver with electromyography signals." Chinese Journal of Mechanical Engineering 3, no. 27 (2014): 460-467.

[26] A. Pick and D. J. Cole, "Dynamic properties of a driver's arms holding a steering wheel," Proceedings of the Institution of Mechanical Engineers, Part D: Journal of Automobile Engineering, vol. 221, pp. 1475-1486, 2007.

[27] C. Lv, Y. Xing, C. Lu, Y. Liu, H. Guo, H. Gao, et al., "Hybrid-Learning-Based Classification and Quantitative Inference of Driver Braking Intensity of an Electrified Vehicle," IEEE Transactions on Vehicular Technology, 2018, in press.

[28] Y. Liu, Q. Liu, C. Lv, M. Zheng, and X. Ji, "A Study on Objective Evaluation of Vehicle Steering Comfort Based on Driver's Electromyogram and Movement Trajectory," IEEE Transactions on Human-Machine Systems, vol. 48, pp. 41-49, 2018.

[29] Liu, Y., Liu, Q., Ji, X., Hayama, R., Mizuno, T. and Nakano, S. A new objective evaluation method for vehicle steering comfort. Journal of Dynamic Systems, Measurement, and Control, 139(9), p.091013, 2017.

[30] L. Ljung. System identification. John Wiley & Sons, Inc., 1999.

[31] Björck, Åke. Numerical methods for least squares problems. Society for Industrial and Applied Mathematics, 1996.

[32] Kelley, Carl T. Iterative methods for optimization. Society for Industrial and Applied Mathematics, 1999.

This article has been accepted for publication in a future issue of this journal, but has not been fully edited. Content may change prior to final publication. Citation information: DOI 10.1109/TMECH.2018.2812643, IEEE/ASME Transactions on Mechatronics

Chen Lv is currently a Research Fellow at Advanced Vehicle Engineering Center, Cranfield University, UK. He received the Ph.D. degree at Department of Automotive Engineering, Tsinghua University, China in 2016. From 2014 to 2015, he was a joint PhD researcher at EECS Dept., University of California, Berkeley. His research focuses on cyber-physical system, hybrid system, advanced vehicle control and intelligence, where he has contributed over 40 papers and holds 11 granted China patents. Dr. Lv serves as a Guest Editor for IEEE/ASME Transactions on Mechatronics and IEEE Transactions on Industrial Informatics, and an Associate Editor for International Journal of Electric and Hybrid Vehicles, International Journal of Vehicle Systems Modelling and Testing, and International Journal of Science and Engineering for Smart Vehicles. He received the Highly Commended Paper Award of IMechE UK in 2012, the NSK Outstanding Mechanical Engineering Paper Award in 2014, the Tsinghua University Graduate Student Academic Rising Star Nomination Award in 2015, the China SAE Outstanding Paper Award in 2015, the 1st Class Award of China Automotive Industry Scientific and Technological Invention in 2015, and the Tsinghua University Outstanding Doctoral Thesis Award in 2016.

Huaji Wang received the B.S. degree in automotive engineering from Jilin University, China, in 2005, and the Ph.D. degree in engineering from the University of Cambridge, Cambridge, U.K., in 2016, concentrating on the study of driver/vehicle systems and driver-automation collaboration. He presently works as a Research Fellow in Automated Driving at Cranfield University, UK.

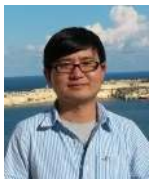

Dongpu Cao received the Ph.D. degree from Concordia University, Canada, in 2008. He was with the Advanced Vehicle Engineering Center, Cranfield University, UK. He is currently an Associate Professor at the Department of Mechanical and Mechatronics Engineering, University of Waterloo, Canada. His research focuses on vehicle dynamics and control, automated driving and parallel driving, where he has contributed more than 100 publications and 1 US patent. He received the ASME AVTT'2010 Best Paper Award and 2012 SAE Arch T. Colwell Merit Award. Dr. Cao serves as an Associate Editor for IEEE TRANSACTIONS ON INTELLIGENT TRANSPORTATION SYSTEMS, IEEE TRANSACTIONS ON VEHICULAR TECHNOLOGY, IEEE TRANSACTIONS ON INDUSTRIAL ELECTRONICS, IEEE/ASME TRANSACTIONS ON MECHATRONICS and ASME JOURNAL OF DYNAMIC SYSTEMS, MEASUREMENT, AND CONTROL. He has been a Guest Editor for VEHICLE SYSTEM DYNAMICS, and IEEE TRANSACTIONS ON HUMAN-MACHINE SYSTEMS. He serves on the SAE International Vehicle Dynamics Standards Committee and a few ASME, SAE, IEEE technical committees.

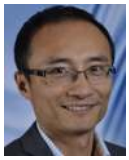

Yifan Zhao was born in Zhejiang, China. He received the Ph.D. degree in automatic control and system engineering from the University of Sheffield, Sheffield, U.K., in 2007. He is currently a Lecturer in image and signal processing and degradation assessment at Cranfield University, Cranfield, U.K. His research interests include computer-vision-based process monitoring, super resolution, active thermography, and nonlinear system identification.

Daniel J. Auger received the M.Eng. and Ph.D. degrees in control engineering from Cambridge University, Cambridge, U.K., specializing in model validation for robust feedback control design. He is currently a Senior Lecturer in Advanced Control and Optimization with Cranfield University, Cranfield, U.K. His recent publications have looked at techniques for addressing battery aging through optimal system design, the development of advanced battery state estimators, and techniques for the quantification of in-vehicle battery degradation. His current research interests include the application of advanced control methodologies to automotive design, development of software-embeddable battery models, optimal state-estimator design, and robust control architectures.

Mark Sullman is currently a Professor of Middle East Technical University, Cyprus. He was a Senior Lecturer based in the Driving Research Group, located in the Department of Advanced Systems. He received MSc and PhD from Massey University, New Zealand. He has more than 20 years of research and consultancy experience in the areas of occupational safety and driving behaviour and has provided consultancy for a number of multinational companies. He is on the Editorial Advisor Board for Transportation Research Part F (Traffic Psychology and Behaviour) and regularly reviews articles for several other international journals. In 2010 he was appointed the European representative for Division 13 of the International Association of Applied Psychology (IAAP) and has been on the Scientific Advisory board for many international conferences. He has authored over 65 journal articles, 24 book chapters, and more than 150 conference papers and industry reports.

Rebecca Matthias is the Capability Research Human Factors Group Leader at Jaguar Land Rover.

Lee Skrypchuk is a Human Machine Interface Technical Specialist at Jaguar Land Rover.

Alexandros Mouzakitis is the Head of Electrical, Electronics & Software Engineering Research Department at Jaguar Land Rover